Article

Excited-State Singlet Manifold and Oscillatory Features of a Nonatetraeniminium Retinal Chromophore Model

Alessandro Cembran, Fernando Bernardi, Massimo Olivucci, and Marco Garavelli

J. Am. Chem. Soc., **2003**, 125 (41), 12509-12519• DOI: 10.1021/ja030215j • Publication Date (Web): 17 September 2003

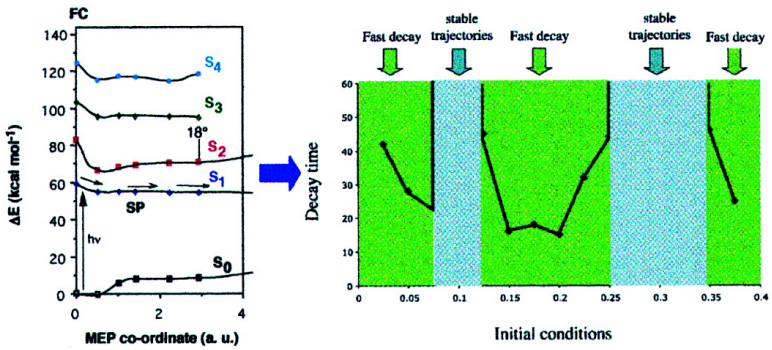

More About This Article

Additional resources and features associated with this article are available within the HTML version:

- Supporting Information
- Links to the 5 articles that cite this article, as of the time of this article download
- Access to high resolution figures
- Links to articles and content related to this article
- Copyright permission to reproduce figures and/or text from this article

View the Full Text HTML

J|A|C|S
ARTICLES
Published on Web 09/17/2003

Excited-State Singlet Manifold and Oscillatory Features of a Nonatetraeniminium Retinal Chromophore Model

Alessandro Cembran,[†] Fernando Bernardi,[†] Massimo Olivucci,*[,‡,§] and Marco Garavelli*[,†]

Contribution from the Dipartimento di Chimica, Università di Siena, via Aldo Moro, Siena, I-53100 Italy, Centro per lo Studio dei Sistemi Complessi, Università di Siena, via Pendola 37, Siena, I-53100 Italy, and Dipartimento di Chimica "G. Ciamician", Università di Bologna, Via Selmi 2, Bologna, I-40126 Italy

Received April 7, 2003; E-mail: mgara@ciam.unibo.it; olivucci@unisi.it

Abstract: In this paper we use ab initio multireference Møller−Plesset second-order perturbation theory computations to map the first five singlet states (S_0, S_1, S_2, S_3, and S_4) along the initial part of the photoisomerization coordinate for the isolated rhodopsin chromophore model 4-*cis*-γ-methylnona-2,4,6,8-tetraeniminium cation. We show that this information not only provides an explanation for the spectral features associated to the chromophore in solution but also, subject to a tentative hypothesis on the effect of the protein cavity, may be employed to explain/assign the ultrafast near-IR excited-state absorption, stimulated emission, and transient excited-state absorption bands observed in rhodopsin proteins (e.g. rhodopsin and bacteriorhodopsin). We also show that the results of vibrational frequency computations reveal a general structure for the first (S_1) excited-state energy surface of PSBs that is consistent with the existence of the coherent oscillatory motions observed both in solution and in bacteriorhodopsin.

1. Introduction

The protonated Schiff base (PSB) of retinal is the chromophore of rhodopsin proteins.[1,2] The biological function of this family of photoreceptors is triggered by the photoinduced isomerization of a specific double bond of the chromophore. In particular, in rhodopsin (Rh), the human retina visual pigment, an 11-cis retinal PSB (PSB11) chromophore is converted into its all-trans form (PSBT). Similarly in bacteriorhodopsin (bR), a photodriven bacterial proton pump, a PSBT chromophore is converted into the 13-cis isomer.

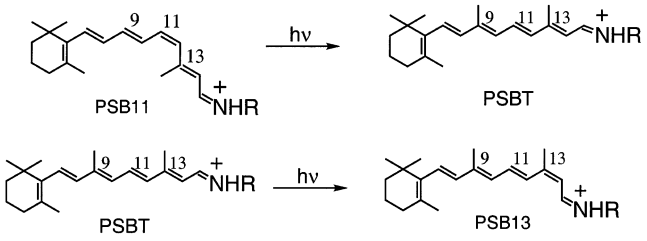

In recent works[3−5] we have shown that the 4-*cis*-γ-methylnona-2,4,6,8-tetraeniminium cation **1** under isolated conditions (i.e. in the absence of a counterion or solvent environment) provides a qualitatively correct model for retinal PSBs photoisomerization.

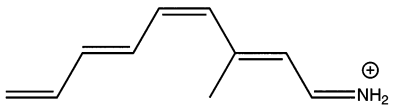

1

The computed ground-state (S_0) and excited-state (S_1) equilibrium structures and energies of **1** have been used to assess the quality of the model with respect to retinal PSBs in hydrocarbon solution. The computed absorption and fluorescence maxima (482 and 594 nm, respectively)[5] compare reasonably well with the experimental absorption maximum for the protonated *N*-butylamine of the retinal Schiff base in hexane (458 nm for both the 11-cis and all-trans forms)[6] and the experimental fluorescence maximum (ca. 620 nm for the all-trans form).[7] Further evidence for the high quality of model **1** comes from a simulation of the PSB11 resonance Raman spectra.[4] Moreover, the computed excited- and ground-state charge distribution has been validated by comparison with the observed dipole moment for the all-trans *N*-butyl retinal PSB

[†] Università di Bologna.
[‡] Dipartimento di Chimica, Università di Siena.
[§] Centro per lo Studio dei Sistemi Complessi, Università di Siena.

(1) Needleman, R. In *CRC Handbook of Organic Photochemistry and Photobiology*; Horspool, W. M., Song, P.-S., Eds.; CRC Press: Boca Raton, FL, 1995; pp 1508−1515.
(2) Ottolenghi, M.; Sheves, M. *Isr. J. Chem.* **1995**, *35*, U3.
(3) Garavelli, M.; Vreven, T.; Celani, P.; Bernardi, F.; Robb, M. A.; Olivucci, M. *J. Am. Chem. Soc.* **1998**, *120*, 1285.
(4) Garavelli, M.; Negri, F.; Olivucci, M. *J. Am. Chem. Soc.* **1999**, *121*, 1023. In this paper we show that resonance Raman spectra computed on the basis of the S_1 and S_0 optimized geometries, gradients, and vibrational frequencies reproduce the details of the observed spectra for PSB11 and its isotopomers in solution.
(5) Gonzalez-Luque, R.; Garavelli, M.; Bernardi, F.; Merchan, M.; Robb, M. A.; Olivucci, M. *Proc. Natl. Acad. Sci. U.S.A.* **2000**, *97*, 9379.
(6) Freedman, K. A.; Becker, R. S. *J. Am. Chem. Soc.* **1986**, *108*, 1245.
(7) Bachilo, S. M.; Bondarev, S. L.; Gillbro, T. *J. Photochem. Photobiol. B, Biol.* **1996**, *34*, 39.

Scheme 1

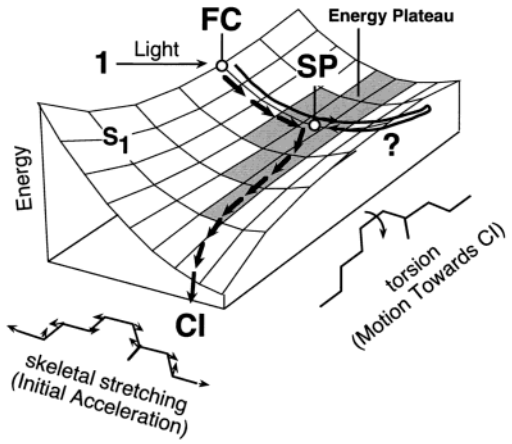

in dioxetane solution.[8] The observed 12.0 D $S_0 \rightarrow S_1$ dipole moment change $|\Delta\mu|$ is of the same magnitude as the 14.0 D value computed for **1**. These data, together with wave function analysis, demonstrate that S_1 has an ionic B_u-like hole-pair (singly excited) character rather then a covalent A_g-like dot-dot (doubly excited) character and, thus, corresponds to the spectroscopic state.[9]

The vacuum photoisomerization coordinate of **1** has also been computed.[3] By using fully unconstrained ab initio quantum-chemical computations in the framework of a CASPT2//CASSCF strategy (i.e., the reaction coordinate is computed at the CASSCF level and the energy profile is reevaluated at the CASPT2 level to take into account the effect of electron dynamic correlation) we have shown that the reaction must occur according to the FC $\rightarrow$ SP $\rightarrow$ CI mechanism illustrated in Scheme 1. The computed minimum energy path (see stream of arrows) connecting the Franck−Condon point (FC) to the S_1/S_0 conical intersection CI defines the excited-state reaction coordinate. This is bimodal. The initial relaxation out of FC is dominated by a symmetric (i.e. planar) stretching mode that leads to a flat planar energy minimum (SP) with an inverted double-bond/single-bond alternation. This deformation is then followed by evolution along a torsional mode dominated by cis $\rightarrow$ trans isomerization motion about the central bond. A remarkable feature of the computed photoisomerization path is that SP lies at the center of an extended energy plateau (shaded area in Scheme 1), which develops along the torsional coordinate and which tends to disappear in shorter chain PSB models.[10,11] This plateau is left only when the torsional angle is >30° and the molecule evolves toward a 90° twisted structure corresponding to CI. We have proposed that this energy plateau corresponds to the picosecond fluorescent state observed for retinal PSBs in solution and that changes in its structure are related to the observed difference in lifetime between the chromophore in solution and in the protein.[12−21]

Despite the fact that the results of quantum-chemical computations have successfully explained certain basic spectral and reaction coordinate features of retinal PSBs, other transient spectral observations[12−26] involving singlet excited states higher than S_1 have not yet been rationalized. For instance, the nature of the S_n state responsible for the 520 nm[19,20] transient $S_1 \rightarrow S_n$ excited-state absorption of PSBT in methanol solution has not been established. Similarly, the competing S_1 near-IR absorption and stimulated emission observed in bR (~850 nm)[22,23] concurrently with $S_1 \rightarrow S_n$ absorption (peaking at 490 nm)[14,15,24−26] have not been rationalized. Finally, the ultrafast S_n decay reported by El-Sayed and co-workers[25] clearly calls for a better knowledge of the structure of the singlet manifold of retinal chromophores.

Other unexplained spectroscopic features regard the motion of the retinal PSBs after their initial relaxation on S_1. One of these is the discovery of a transient damped low-frequency oscillatory feature in the stimulated emission spectra, which has been tentatively assigned to the chromophore S_1 dynamics[27−30] (i.e., these modulations have been associated with vibrational coherences in the excited state). This behavior appears to be general. In fact, the same type of spectral oscillations has been observed for PSBT in solution (117 cm^{-1}) and in the bR protein (156 cm^{-1}). Remarkably, the same feature is present in different locked retinal PSB derivatives (both in solution and in the protein, see below),[27−30] where the isomerization motion is hindered. While these features are suggestive of a complex S_1 dynamics, no mechanistic model has been presently proposed for their origin and decay.

(8) Mathies, R.; Stryer, L. *Proc. Natl. Acad. Sci. U.S.A.* **1976**, *73*, 2169.
(9) One possible reason for the success of model **1** is that retinal PSBs have a ca. 60° twisted 6-s-cis conformation of the β-ionone ring in their equilibrium geometry in solution, according to H^1 NMR NOE experiments (see Albeck, A.; Livnah, N.; Gottlieb, H.; Sheves, M. *J. Am. Chem. Soc.* **1992**, *114*, 2400) and recent computational investigations (see Rajamani, R.; Gao, J. *J. Comput. Chem.* **2001**, *23*, 96). The same situation also appears in the crystallographic structure of Rh for its PSB11 chromophore (see Teller, D. C.; Okada, T.; Behnke, C. A.; Palczewski, K.; Stenkamp, R. E. *Biochemistry* **2001**, *40*, 7761−7772). This prevents efficient conjugation of the β-ionone double bond with the rest of the conjugated chain, making **1** a realistic model for retinal PSBs, at least under isolated conditions.
(10) Garavelli, M.; Celani, P.; Bernardi, F.; Robb, M. A.; Olivucci, M. *J. Am. Chem. Soc.* **1997**, *119*, 6891.
(11) Garavelli, M.; Bernardi, F.; Olivucci, M.; Vreven, T.; Klein, S.; Celani, P.; Robb, M. A. *Faraday Discuss.* **1998**, *110*, 51.
(12) Chosrowjan, H.; Mataga, N.; Shibata, Y.; Tachibanaki, S.; Kandori, H.; Shichida, Y.; Okada, T.; Kouyama, T. *J. Am. Chem. Soc.* **1998**, *120*, 9706.
(13) Kakitani, T.; Akiyama, R.; Hatano, Y.; Imamoto, Y.; Shichida, Y.; Verdegem, P.; Lugtenburg, J. *J. Phys. Chem. B* **1998**, *102*, 1334.
(14) Mathies, R. A.; Cruz, C. H. B.; Pollard, W. T.; Shank, C. V. *Science* **1988**, *240*, 777.
(15) Dobler, J.; Zinth, W.; Kaiser, W.; Oesterhelt, D. *Chem. Phys. Lett.* **1988**, *144*, 215.
(16) Schoenlein, R. W.; Peteanu, L. A.; Mathies, R. A.; Shank, C. V. *Science* **1991**, *254*, 412.
(17) For a survey of the photochemistry and photophysics of model retinal chromophores in solution see: Becker, R. S. *Photochem. Photobiol.* **1988**, *48*, 369.
(18) Kandori, H.; Katsuta, Y.; Ito, M.; Sasabe, H. *J. Am. Chem. Soc.* **1995**, *117*, 2669.
(19) Logunov, S. L.; Song, L.; ElSayed, M. A. *J. Phys. Chem.* **1996**, *100*, 18586.
(20) Hamm, P.; Zurek, M.; Roschinger, T.; Patzelt, H.; Oesterhelt, D.; Zinth, W. *Chem. Phys. Lett.* **1996**, *263*, 613.
(21) Kandori, H.; Sasabe, H. *Chem. Phys. Lett.* **1993**, *216*, 126.
(22) Hasson, K. C.; Gai, F.; Anfinrud, P. A. *Proc. Natl. Acad. Sci. U.S.A.* **1996**, *93*, 15124.
(23) Gai, F.; Hasson, K. C.; McDonald, J. C.; Anfinrud, P. A. *Science* **1998**, *279*, 1886.
(24) Haran, G.; Morlino, E. A.; Matthes, J.; Callender, R. H.; Hochstrasser, R. M. *J. Phys. Chem. A* **1999**, *103*, 2202. $S_1 \rightarrow S_n$ transition dipoles have been recorded for Rh. Their direction is a function of the geometry of the chromophore in space. While in Rh the chromophore is highly twisted, chromophore model **1** used in our computations is planar. This may affect quantitatively the value of the computed transition dipole directions, making comparison with the observed values not strictly correct. Still, we believe that the behavior and progress of transition dipole directions along the path is qualitatively reproduced, allowing a qualitative comparison with experiments.
(25) Logunov, S. L.; Volkov, V. V.; Braun, M.; El-Sayed, M. A. *Proc. Natl. Acad. Sci. U.S.A.* **2001**, *98*, 8475.
(26) Sharkov, A. V.; Pakulev, A. V.; Chekalin, S. V.; Matveets, Y. A. *Biochim. Biophys. Acta* **1985**, *808*, 94.
(27) Hou, B.; Friedman, N.; Ruhman, S.; Sheves, M.; Ottolenghi, M. *J. Phys. Chem. B* **2001**, *105*, 7042.
(28) Ye, T.; Friedman, N.; Gat, Y.; Atkinson, G. H.; Sheves, M.; Ottolenghi, M.; Ruhman, S. *J. Phys. Chem. B* **1999**, *103*, 5122.
(29) Ye, T.; Gershgoren, E.; Friedman, N.; Ottolenghi, M.; Sheves, M.; Ruhman, S. *Chem. Phys. Lett.* **1999**, *314*, 429.
(30) Zinth, W. Personal communication.

In the present work we use the PSB11 model **1** to collect information on the higher excited states (S_2, S_3, and S_4) of retinal PSBs *in general*. This means that **1** will not be used to interpret the behavior of PSB11 or Rh exclusively but will be taken as a general retinal chromophore model and used for a substantially qualitative analysis of the spectroscopic features described above. Multireference Møller−Plesset second-order perturbation theory is employed to compute the energy of the first five singlet states (S_0, S_1, S_2, S_3, and S_4) along the initial part (i.e. up to a 18° torsional deformation) of the photoisomerization path seen in Scheme 1. The values for the $S_0 \rightarrow S_1$, $S_1 \rightarrow S_2$, $S_1 \rightarrow S_3$, and $S_1 \rightarrow S_4$ energies, oscillator strengths, and transition dipole moments along the path are reported. We show that such information supports a potential energy surface (PES) topography consistent with the observed transient excited-state absorption of retinal PSBs both in solution and, subject to a tentative hypothesis on the effect of the opsin cavity, in retinal proteins. The same effect would account for the near-IR excited-state absorption observed in Rh and bR.

To collect information on the mechanism of $S_2 \rightarrow S_1$ internal conversion (i.e. on the efficiency of the decay from an upper to a lower singlet excited state), the relationship between the S_1 and S_2 PESs of model **1** is explored. The computed data support a mechanism involving a fully efficient decay through a S_2/S_1 conical intersection that has never been documented before in PSBs and may, in principle, constitute a common feature in systems where the Kasha rule for decay from upper excited states successfully applies.

Finally, to provide a computationally based mechanistic explanation for the observed damped nonperiodic coherent oscillations in excited-state retinal PSBs, the topography of the S_1 PES in its Franck−Condon region has been characterized via computation and analysis of the S_1 vibrational frequencies of model **1**. It is shown that three low-frequency vibrational modes exist in this region that may correspond to the 117 cm^{-1} oscillation observed for PSBT in ethanol solution.[27] A crude but topographically correct analytical model of the same PES has then been employed to investigate the character of the early dynamics of a vibrational wave packet. We demonstrate that the surface topography in this region induces both nonperiodic oscillations of the wave packet and an evolution out of the Franck−Condon region characterized by at least two different regimes that provide an alternative explanation/assignment to the observed biexponential decay in solution.[20]

2. Computational Methods

The singlet manifold (ground state—S_0—and first four singlet excited states—S_1, S_2, S_3, and S_4) energetics has been computed at the ab initio multireference-MP2 level (using the CASPT2 method included in MOLCAS-5)[31] with the 6-31G* basis set. To describe the sensitivity of the energy separation to the change in molecular structure, the S_0−S_4 energies are reported *along the initial part of the previously determined*[3] *S_1 photoisomerization coordinate* for the PSB11 model **1**. A complete active space of 10 π-electrons in 10 π-orbitals (10e/10o) and single-root computations were used to describe the zeroth order CASSCF wave function in all cases. Dipole moments and charge distribution (Mulliken charges[5,10,32]) along the backbone of **1** were determined at the CASSCF 10e/10o level of theory. To assess the efficiency and probability for radiative transition among these states, the RASSI (restricted active space state interaction) approach[33] has been used to compute the oscillator strength (f) of vertical electronic transitions along the path.[34] Orientations of the computed $S_0 \rightarrow S_1$, $S_1 \rightarrow S_2$, $S_1 \rightarrow S_3$, and $S_1 \rightarrow S_4$ electronic transition dipole moments with respect to their initial (FC) direction have also been reported for some selected points along the photoisomerization path.

To accurately determine the S_1 PES topography responsible for the initial excited-state dynamics, CASSCF (10e/10o) numerical frequency computations have been performed at the previously reported[3,5] stationary point SP. These parts of the computations have been carried out using the Gaussian98 package.[35] The same package has been used to locate the equilibrium structure on the S_2 state. With this structure as a starting point, a planar S_1/S_2 conical intersection structure has been located by scanning the S_2 energy surface along the S_1-S_2 gradient difference vector that defines the direction of the fastest decrease in S_2-S_1 energy gap. The energetics along the scan has then been determined by correcting the (S_1, S_2) two-roots state-averaged CASSCF results with single-point CASPT2 computations.

3. Results and Discussion

In Table 1 and Figure 1 we report the S_0, S_1, S_2, S_3, and S_4 energies of six points along the initial part (i.e. from 0 to 18° torsional deformation) of the S_1 reaction coordinate (see stream of arrows in Figure 1). In Table 2 we report the corresponding dipole moments and charge distributions at the S_1 relaxed planar structure SP. As previously described,[5] a positive-charge translocation from the nitrogen head to the hydrocarbon tail of the chromophore is prompted upon the $S_0 \rightarrow S_1$ transition that reflects the change in the nature of the electronic wave function. In contrast, almost no charge translocation is predicted for the alternative $S_0 \rightarrow S_n$ transitions (i.e. when $n = 2-4$). These results are consistent with the fact that S_1 is the only state dominated by a hole-pair character (i.e., it is an ionic B_u-like state). The remaining excited states display a covalent (A_g-like) dot-dot character. As a consequence, transitions from S_1 to S_0 (emission) or from S_1 to S_2, S_3, and S_4 (absorption) are, in principle, allowed. On the other hand, according to our results the $S_0 \rightarrow S_1$ transition has an oscillator strength at least 1 order of magnitude larger than the other $S_1 \rightarrow S_n$ excited-state transitions (see Table 3).

3.1. Spectral Features in Solution and in the Protein. As already noted,[3−5] the computed absorption and fluorescence maxima (481 and 602 nm, respectively; see Figure 1) agree

(31) Andersson, K.; Blomberg, M. R. A.; Fülscher, M. P.; Karlström, G.; Lindh, R.; Malmqvist, P.-Å.; Neogrády, P.; Olsen, J.; Roos, B. O.; Sadlej, A. J.; Schütz, M.; Seijo, L.; Serrano-Andrés, L.; Siegbahn, P. E. M.; Widmark, P.-O. MOLCAS-5; Lund University: Lund, Sweden, 1999.

(32) In a previous work on a shorter PSB11 model (i.e. the penta-3,5-dieniminium cation) we demonstrated that, for this system, the atomic charges computed using different schemes (NPA, CHelpG, MKS) yield the same charge distribution.[10] Moreover, in ref 5 we showed that Mulliken and NBO charges give the same results.

(33) Malmqvist, P.-Å.; Roos, B. O. *Chem. Phys. Lett.* **1989**, *155*, 189.

(34) RASSI[33] has been used to compute the transition dipole moments (TMD) from the CASSCF reference wave functions. The oscillator strength (f) is defined as $f = {}^2/_3|M_{if}|^2(\Delta E_{fi})$, where M_{if} is the TMD (in au) and ΔE_{fi} is the CASPT2 excitation energy (in au).

(35) Frisch, M. J.; Trucks, G. W.; Schlegel, H. B.; Scuseria, G. E.; Robb, M. A.; Cheeseman, J. R.; Zakrzewski, V. G.; Montgomery, J. A., Jr.; Stratmann, R. E.; Burant, J. C.; Dapprich, S.; Millam, J. M.; Daniels, A. D.; Kudin, K. N.; Strain, M. C.; Farkas, O.; Tomasi, J.; Barone, V.; Cossi, M.; Cammi, R.; Mennucci, B.; Pomelli, C.; Adamo, C.; Clifford, S.; Ochterski, J.; Petersson, G. A.; Ayala, P. Y.; Cui, Q.; Morokuma, K.; Malick, D. K.; Rabuck, A. D.; Raghavachari, K.; Foresman, J. B.; Cioslowski, J.; Ortiz, J. V.; Stefanov, B. B.; Liu, G.; Liashenko, A.; Piskorz, P.; Komaromi, I.; Gomperts, R.; Martin, R. L.; Fox, D. J.; Keith, T.; Al-Laham, M. A.; Peng, C. Y.; Nanayakkara, A.; Gonzalez, C.; Challacombe, M.; Gill, P. M. W.; Johnson, B. G.; Chen, W.; Wong, M. W.; Andres, J. L.; Head-Gordon, M.; Replogle, E. S.; Pople, J. A. *Gaussian 98*, revision A.6; Gaussian, Inc.: Pittsburgh, PA, 1998.

Table 1. S_0, S_1, S_2, S_3, and S_4 Single-State CASSCF and Multireference-MP2 (PT2) Absolute and Relative (ΔE) Energies for the PSB11 Model 1 (6-31G* Basis Set)

	state	CASSCF, au	PT2, au	ω[a]	ΔE, eV (kcal mol^{-1})
0.0 au	S_0	−441.130 38	−442.430 89	0.70	0.00 (0.00)
planar FC	S_1	−440.998 77	−442.336 22	0.68	2.58 (59.4)
	S_2	−440.961 73	−442.298 15	0.68	3.61 (83.3)
		−440.971 21 (CAS10−11)[b]	−442.296 91 (CAS10−11)[b]	0.69	[0.00 (0.00)][c]
	S_3	−440.924 51	−442.271 13	0.04[b]	
		−440.934 13 (CAS10−11)[b]	−442.263 31 (CAS10−11)[b]	0.65	[0.91 (21.03)][c]
			{442.264 55}[c]		4.53 (104.4)
	S_4	−440.893 91	−442.230 56	0.68	5.45 (125.7)
0.5 au	S_0	−441.121 41	−442.432 02	0.69	−0.03 (−0.7)
	S_1	−441.008 20	−442.344 27	0.68	2.36 (54.4)
		−441.004 14 (SA)	−442.348 46 (SA)	0.68	[0.00 (0.00)][c]
	S_2[d]	−440.984 51 (SA)	−442.327 59 (SA)	0.68	[0.57(13.1)][c]
			{−442.3234}[c]		2.92 (67.4)
	S_3	−440.944 03	−442.277 49	0.66	4.17 (96.3)
	S_4	−440.910 68	−442.245 33	0.68	5.05 (116.4)
1.0 au	S_0	−441.101 90	−442.421 25	0.69	0.26 (6.05)
	S_1	−441.011 61	−442.343 14	0.69	2.39 (55.1)
	S_2	−440.981 78	−442.321 58	0.68	2.97 (68.6)
	S_3	−440.944 81	−442.276 28	0.48[e]	4.21 (97.0)
	S_4	−440.910 02	−442.243 01	0.68	5.11 (117.9)
1.4 au	S_0	−441.098 48	−442.418 79	0.69	0.33 (7.6)
planar SP	S_1	−441.012 01	−442.343 06	0.69	2.39 (55.1)
		−441.008 04 (SA)	−442.349 95 (SA)	0.68	[0.00 (0.00)][c]
	S_2	−440.979 31	−442.319 24	0.68	3.04 (70.1)
		−440.975 95 (SA)	−442.320 39 (SA)	0.68	[0.80 (18.5)][c]
	S_3	−440.944 32	−442.277 75	0.55[e]	4.17 (96.1)
	S_4	−440.909 41	−442.242 16	0.68	5.14 (118.4)
2.20 au	S_0	−441.097 35	−442.418 17	0.69	0.35 (8.0)
	S_1	−441.012 31	−442.343 53	0.69	2.38 (54.8)
	S_2	−440.978 10	−442.318 30	0.68	3.06 (70.7)
	S_3	−440.944 39	−442.278 01	0.50[e]	4.16 (95.9)
	S_4	−440.908 99	−442.241 41	0.66	5.16 (118.9)
2.90 au	S_0	−441.095 84	−442.417 05	0.69	0.38 (8.7)
	S_1	−441.012 65	−442.343 90	0.69	2.37 (54.6)
	S_2	−440.976 81	−442.317 24	0.68	3.09 (71.3)
	S_3	−440.944 70	−442.278 14	0.48[e]	4.15 (95.9)
	S_4	−440.909 03	−442.240 82	0.67	5. 17 (119.27)
44°	S_0	−441.082 91	−442.406 43	0.69	0.67 (15.35)
	S_1	−441.018 16[f]	−442.350 27	0.69	2.19 (50.59)
	S_2	−440.966 38[f]	−442.307 33	0.58[e]	3.36 (77.53)
68°	S_0	−441.066 35	−442.385 43	0.69	1.24 (28.5)
	S_1	−441.026 34[f]	−442.360 32	0.69	1.92 (44.3)
	S_2	−440.958 63[f]	−442.288 02	0.61[e]	3.89 (89.65)
MIN S2	S_0	−441.110 66	−442,422 83	0.69	0.22 (5.06)
	S_1	−441.002 56	−442,337 53	0.68	2.54 (58.58)
		−440.998 16 (SA)	−442.342 88 (SA)	0.68	[0.00 (0.00)][c]
	S_2[d]	−440.991 34 (SA)	−442.332 20 (SA)	0.68	[0.29 (6.70)][c]
			{−442.326 85}[c]		2.83 (65.28)
CI S1/S2	S_0	−441.083 12	−442.392 97	0.69	1.03 (23.79)
	S_1	−440.964 60 (SA)	−442.312 07 (SA)	0.68	[0.84 (19.33)][c]
			{−442.30672}[c]		3.38 (77.92)
	S_2[d]	−440.971 99 (SA)	−442.311 91 (SA)	0.68	[0.84 (19.43)][c]
			{−442.306 56}[c]		3.38 (78.02)

[a] Weight of the CASSCF reference function (i.e. the zeroth-order function) in the first-order function. [b] In one case the reference weight is too small (0.04), thus calling for a larger active space computation CAS (10e/11o) to correct for intruder states. For comparative purposes, also the PT2F energy of the lower lying state has been computed at this level. The extension (CAS10−11) has been used in the table closed to the corresponding energy values.[c] ΔE data in brackets refer to the same energy type. Absolute energies in braces are estimated (not computed) values based on energy differences, thus allowing a single coherent set of relative energies (ΔE) to be plotted. [d] The CASSCF single state fails for root S_2 due to convergence problems (root flipping). The S_1-S_2 state-averaged (SA) value has been used instead (0.5 weight each). For comparative purposes, also the S_1 PT2F energy has been computed on the basis of the SA CASSCF zeroth-order function. This allows a single coherent set of energy data (both absolute and relative) to be estimated. [e] In a few cases, due to the occurrence of intruder states, the reference weight is smaller than 0.7 (~0.5). In any event, their perturbative energy contribution is very small (<0.5 kcal/mol) and new CASSCF computations (not shown) with larger active spaces gave exactly the same results but normal weights. It is concluded that, despite the low weights, the corresponding results can be confidently used. [f] A level shift (LS) has been used to avoid CASSCF root flipping. Energies appear to be invariant with respect to the LS value used (LS = 2−4).

qualitatively with the experimentally available data (458 and 620 nm, respectively) for the protonated *N*-butylamine of the retinal Schiff base in hexane.[6,7] On the other hand, a transient visible excited state (S_1) absorption has been observed for PSBT in methanol solution in the range 460−575 nm, peaking around 520 nm,[19,20] which, in principle, could be due to either a $S_1 \rightarrow$

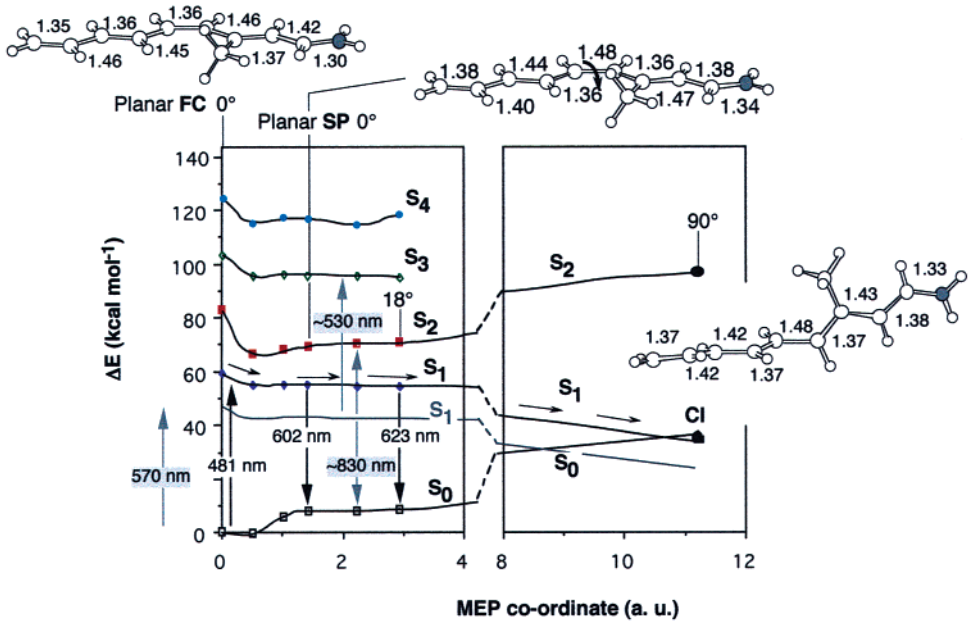

Figure 1. CASPT2 energy profiles for the electronic S_0, S_1, S_2, S_3, and S_4 states along the initial S_1 photoisomerization *two-mode* coordinate[3−5] of the PSB11 model **1**. The structures (geometrical parameters in angstroms and degrees) document the progression of the molecule along the coordinate (in mass-weighted atomic units) and are taken from ref 5. FC is the Franck−Condon structure (S_0 minimum), SP is the planar fully relaxed stationary point on S_1, and CI is the real S_0/S_1 crossing (conical intersection) structure. Solid diamonds show the S_1 energy profile. Open and solid squares, open diamonds, and solid circles show the S_0, S_2, S_3, and S_4 CASPT2 energy cross-sections along the same coordinate, respectively. The shaded line represents a hypothetical opsin-shifted S_1 reaction path.

Table 2. S_0, S_1, S_2, S_3, and S_4 CASSCF Dipole Moments (μ) and Mulliken Charge Distributions at the SP Structure

	μ[a]			charge distribn[b]									
state	*X*	*Y*	*Z*	C_9	C_8	C_7	C_6	C_5	C_4	C_3	C_2	C_1	N
S_0	3.602	1.619	0.0	0.05	0.05	0.07	0.02	0.09	−0.03	0.22	−0.06	0.45	0.14
S_1	.867	.445	0.0	0.14	0.07	0.14	0.05	0.07	−0.01	0.13	−0.01	0.35	0.07
S_2	3.130	1.432	0.0	0.07	0.09	0.03	0.10	0.0	0.04	0.11	0.02	0.39	0.14
S_3	4.665	2.259	0.0	0.01	0.05	0.03	0.04	0.01	0.05	0.21	0.01	0.39	0.19
S_4	4.597	2.283	0.0	0.0	0.05	0.02	0.08	0.02	0.07	0.18	−0.01	0.42	0.17

[a] *X*, *Y*, and *Z* components given in Bohr electrons (au). [b] Charges (in electron units) along the molecular backbone of the planar SP structure.

Table 3. Computed Oscillator Strengths[a] for Radiative Transitions (absorption/emission) at Selected Points along the S_1 Photoisomerization Path[b]

transitions to (→)	FC	SP	18°	44°	68°
→ S_0		1.0469 (5)	1.0011 (2)	0.7591 (3)	0.2445 (3)
→ S_1	0.8334				
→ S_2	0.1969	0.1088 (10)	0.1278 (7)	0.2315 (7)	0.1572 (6)
→ S_3	0.0319	0.0756 (17)	0.0782 (19)		
→ S_4	0.0026	0.0244 (11)	0.0162 (16)		

[a] See ref 33. [b] While the values reported at the FC point correspond to transitions (i.e. absorption) from S_0 to the upper singlet states (S_1, S_2, S_3, and S_4), all other values refer to transitions from S_1 to S_0 (i.e. emission) and from S_1 to higher states (i.e. absorption). The values reported in parentheses give the changes (in degrees) of the corresponding transition dipole direction with respect to its original direction at the FC point.

S_3 or a $S_1 \rightarrow S_4$ allowed transition. While the $S_1 \rightarrow S_3$ transition features a larger value of the oscillator strength (see Table 3), the corresponding S_1-S_3 energy gap is too small (with an absorption maximum of about 700 nm at the SP point) to explain the observed absorption. However, the second transition (with an absorption maximum of about 450 nm) features an energy gap much closer to the observed one and it is thus tentatively assigned to the absorbing state. Notice that at wavelengths shorter than 460 nm a negative signal is observed in the transient absorption spectra, which is attributed to bleaching of the ground-state species. Since our computations indicate that the oscillator strength of the $S_0 \rightarrow S_1$ transition is larger than that of the $S_1 \rightarrow S_4$ transition, the true excited-state absorption maximum in solution may be blue-shifted with respect to the observed maximum (520 nm), as suggested by our computations (450 nm).

While the simulated data provide a basis for the interpretation of the spectral features of PSB11 and PSBT in solution,[3−5,11] one can also attempt to use these data to rationalize the ultrafast spectral changes observed in the protein environment. As mentioned above, our computations show that, while the S_1 state maintains a charge-transfer (hole-pair B_u-like) character all along the *two-mode* reaction coordinate (which is even reinforced proceeding toward the region of the real S_0/S_1 crossing)[3−5] the four S_0, S_2, S_3, and S_4 electronic states preserve a prevalent covalent diradical (dot-dot A_g-like) character.[36,37] This information can be used for a rationalization of the near-IR excited-state absorption and stimulated emission observed in bR[22,23]

(36) Michl, J.; Bonacic-Koutecky, V. *Electronic Aspects of Organic Photochemistry*; Wiley: New York, 1990.

(37) Because of the symmetry being lower than in planar polyenes due to the replacement of a CH_2 group of a polyene with a $NH_2(+)$ group, the S_1 and S_2 states of planar PSBs have a mixed $1B_u/2A_g$ character. Nevertheless, the S_1 state is dominated by the ionic $1B_u$ character, while the S_2 state is dominated by the covalent $2A_g$ character (as it happens for S_0, S_3, and S_4 states); see Tables 2 and 3.

(peaking at ~850 and ~810 nm, respectively). The observation of competing excited state near-IR absorption and stimulated emission implies that in the flat energy region centered on SP (i.e., the region of the fluorescent state), the energy gap between the S_1 and S_2 states is close to the energy gap between the S_1 and S_0 states. In Figure 1 we show that this is not the case for model **1** under isolated conditions, where the S_1-S_0 separation appears to be larger than the S_1-S_2 separation. Nevertheless, we know that, in bR, the protein cavity induces a ~100 nm red shift to the absorption maximum (the so-called *opsin shift*).[1,2] Given the similarity of the charge distributions of the S_2 (S_3, S_4) and S_0 states (these are covalent states: see Table 2 and also ref 5), one expects that the opsin shift would mainly affect the position of the ionic S_1 state (relative to S_0) rather than that of S_2 (S_3, S_4) (relative to S_0 as well). In this case, one may imagine a situation where similar S_1-S_2 and S_1-S_0 energy gaps exist in the SP region after a suitable energy correction has been applied. In fact, correcting (relative to S_0) the S_1 energy profile for the ~100 nm red shift observed in bR,[1,2] one gets close S_1-S_2 and S_1-S_0 gaps in the 800−900 nm range. A ~830 nm S_1-S_0 energy gap in the SP region (i.e. along the energy plateau that is supposed to correspond to the emitting state) is in qualitative agreement with the observed near-IR stimulated emission.[38] Using a similar correction, the manifold computed for **1** suggests that the covalent S_3 state is responsible for the S_1 absorption. Thus, the ~490 nm absorption band observed in bR[25,26] may be assigned to the computed $S_1 \rightarrow S_3$ transition (~530 nm around the SP region, with decreasing wavelength going toward more twisted configurations along the energy plateau).[38,39]

3.2. $S_1 \rightarrow S_n$ Transition Dipole Direction. To predict the changes in the direction of the transition dipole along the S_1 branch of the isomerization path, this quantity has been computed for the $S_0 \rightarrow S_1$, $S_1 \rightarrow S_2$, $S_1 \rightarrow S_3$, and $S_1 \rightarrow S_4$ transitions for a selected number of points along the reaction coordinate. In Table 3 we show that the change in direction (with respect to the direction at FC) for the $S_0 \rightarrow S_1$ and $S_1 \rightarrow S_2$ transitions is very limited. In contrast, the $S_1 \rightarrow S_3$ and $S_1 \rightarrow S_4$ transitions display a significant change in the direction of the transition dipole. This change is mainly due to the nature of the electronic rearrangement occurring along the reaction coordinate and appears to increase upon increasing the torsional deformation. Hochstrasser and co-workers[24] have observed in Rh (by means of S_1 absorption anisotropy measurements at 580 nm) an anisotropy change of 30° occurring in the very initial part of the isomerization process (≤40 fs), which has been tentatively explained by either a change in the electronic wave function (e.g. a sudden charge movement accompanying the $S_1 \rightarrow S_n$ excitation responsible for the excited-state absorption) or the presence of competing transient absorptions. Our computations show that the $S_1 \rightarrow S_3$ and $S_1 \rightarrow S_4$ transitions are consistent with a change in the transition dipole direction on the same order of magnitude of the observed one. This result reinforces the hypothesis that the excited-state absorption in rhodopsin proteins comes from the S_3 or S_4 states.

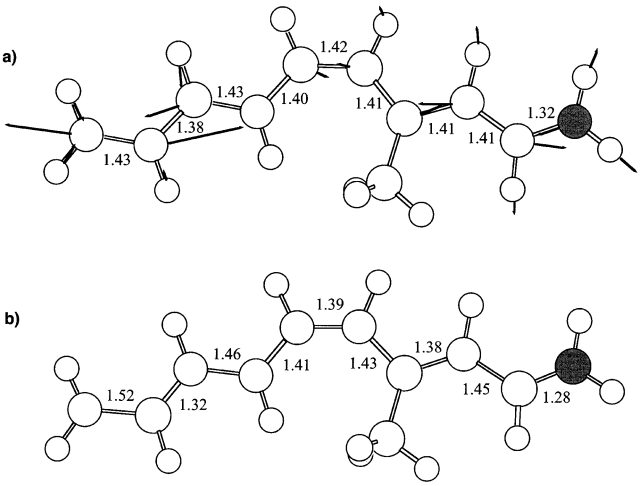

Figure 2. Structures for (a) the optimized planar S_2 minimum (MIN S_2) and (b) the planar S_1/S_2 conical intersection (geometrical parameters in Å). The arrows display the direction of the gradient difference vector (between S_1 and S_2) computed at the S_2 minimum.

3.3. S_2 Equilibrium Structure and S_1-S_2 Internal Conversion. Geometry optimization of **1** on the second excited state, S_2, has been performed to assess the interplay between the S_2 and S_1 energy surfaces and the possible mechanism for $S_1 \rightarrow S_2$ "uphill" internal conversion. The S_2 relaxed structure (MIN S_2) and the corresponding energies are reported in Figure 2a and Table 1, respectively. The S_2 planar minimum displays a diradical (covalent) character with the positive charge located along the nitrogen-containing moiety. The backbone displays a geometry which is consistent with that found for the structures of long-chain conjugated polyenes on their covalent ($2A_g$) excited state S_1.[40−43] In fact, all the internal C−C bonds are similar in length (around 1.41 Å), regardless of their initial single- or double-bond character. While the S_1-S_2 energy gap is quite large at SP (~18 kcal mol^{-1}), this reduces to ~7 kcal mol^{-1} at MIN S_2 (which lies ~11 kcal mol^{-1} higher than the SP point on S_1). With MIN S_2 as the starting point, a displacement along the S_1/S_2 gradient difference vector (see arrows in Figure 2a) leads to a real crossing (i.e. an S_1/S_2 conical intersection) between the S_1 and S_2 energy surfaces[44] (Figure 2b). This is located ~12 kcal mol^{-1} higher than MIN S_2 and ~23 kcal mol^{-1} higher than SP (Figure 3).

These findings support a photoisomerization path that fully lies along the ionic S_1 state, from the FC point to the CI funnel. In fact, $S_1 \rightarrow S_2$ internal conversion (i.e. population of S_2 through relaxation on S_1) is unlikely to occur due to the energy barrier to reach the S_1/S_2 conical intersection. If **1** is vertically excited

(38) S_1 fluorescence as well as S_1 absorption maxima (481 and 602 nm, respectively) have been obtained by assuming that the fluorescent/absorbing S_1 state is dominated by planar or slightly twisted configurations and is localized along the very initial part of the S_1 energy plateau of Figure 1 (centered on SP). Population of more twisted configurations along the plateau would increase (decrease) the wavelength of the fluorescent (absorption) maxima. Thus, the predicted fluorescence value under isolated conditions is 623 nm for a 18° twisted structure, and ~830 nm after scaling by the observed opsin shift in bR (112 nm = 570 nm − 458 nm).

(39) All these spectral features (intense excited-state absorption and near-IR stimulated emission) show a surprisingly short rise time (30 fs for bR[29] and 50 fs for Rh[24]), thus suggesting that the previously reported 100 fs time scale[14,15] for the production of the fluorescent state in bR may be overestimated.

(40) Garavelli, M.; Celani, P.; Bernardi, F.; Robb, M. A.; Olivucci, M. *J. Am. Chem. Soc.* **1997**, *119*, 11487.
(41) Garavelli, M.; Smith, B. R.; Bearpark, M. J.; Bernardi, F.; Olivucci, M.; Robb, M. A. *Abstr. Pap. Am. Chem. Soc.* **1999**, *217*, U301.
(42) Garavelli, M.; Celani, P.; Yamamoto, N.; Bernardi, F.; Robb, M. A.; Olivucci, M. *J. Am. Chem. Soc.* **1996**, *118*, 11656.
(43) Celani, P.; Garavelli, M.; Ottani, S.; Bernardi, F.; Robb, M. A.; Olivucci, M. *J. Am. Chem. Soc.* **1995**, *117*, 11584.
(44) The search and optimization of a S_1/S_2 conical intersection by the standard algorithm has not been successful, due to wave function convergence problems in that PES region; therefore, the conical intersection we found is not the lowest energy one.

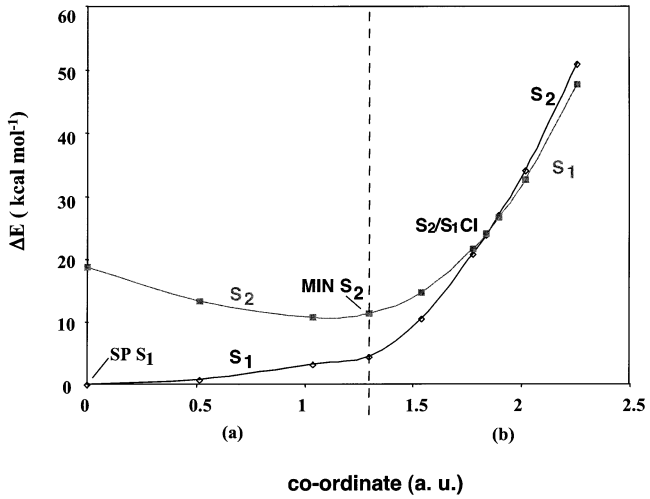

Figure 3. CASPT2 energy profiles for the electronic S_1 and S_2 states along the linear paths (in mass-weighted atomic units) connecting (a) MIN S_2 to SP (following an interpolated coordinate) and (b) MIN S_2 to the S_1/S_2 CI conical intersection (following the gradient difference vector of Figure 2a). Note that these two directions are almost perpendicular to each other (96°).

to S_1 with no vibrational excess energy, it will gain about 5 kcal mol^{-1} of kinetic energy by relaxing from FC to SP. This is much less than the energy required to hit the conical intersection (∼23 kcal mol^{-1}). In contrast, the existence of a S_1/S_2 conical intersection decay channel suggests that "downhill" $S_2 \rightarrow S_1$ internal conversion may take place when decaying from higher energy excited states. Of course, the 12 kcal mol^{-1} barrier that must be overcome can restrain efficient internal conversion. However, this is only an upper limit.[44] Furthermore, one has to consider that since the S_2 state is populated by decay from higher excited states (consistent with the experiment),[25] the excess vibrational energy gained through relaxation from the initially populated S_n state is likely to provide enough energy to overcome the barrier to the conical intersection. Finally, it must be outlined that the dynamics of the molecule on the S_1 surface may be different if the surface is populated from above, rather than directly from the ground-state surface. New minimum energy path computations or dynamics simulations on higher energy excited states are necessary to properly answer this point.

The discovery of a conical intersection between the S_2 and the S_1 states suggests that higher singlet excited states may potentially be connected to the lowest singlet excited state via a series of conical intersections, as illustrated in Scheme 2. The existence of such features would provide a mechanistic model consistent with the result of the El-Sayed experiment[25] and with the validity of the Kasha rule.[45] In other words, a chromophore promoted to an upper singlet state S_n could rapidly (i.e. ultrafast time scale) decay to S_1 when a series of consecutive intersections are accessed along an energetically favored (e.g. barrierless) relaxation path. On the other hand, in a chromophore that does not obey the Kasha rule (e.g. azulene), fast decay from an upper to a lower singlet state can be restrained when a nonnegligible energy barrier exists along the path to the conical intersection. Although this seems to apply to **1**, the computed energy barrier is an upper limit and should be much smaller than the S_2 excess vibrational energy available after S_n relaxation. Although this is nothing but a speculative hypothesis (which needs to be proved by additional computational investigations), we still think it is a reasonable suggestion, providing a straightforward rational for the experiments reported in ref 25.

Scheme 2

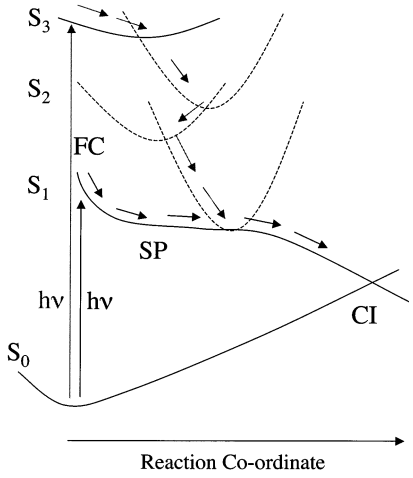

3.4 Coherent Oscillations on S_1. In this section we focus on the problem of determining the nature of the photoinduced coherent wave packet oscillatory motion observed in both bR and solution PSBT by Ottolenghi, Ruhman, and co-workers[27−29,46] and in bR by Zinth and co-workers.[30] This is revealed by damped oscillatory modulations of the stimulated emission signal. Assuming (see below) that the structure of the S_1 potential energy surface of bR and PSBT in solution is structurally similar to that of the PSB11 model **1**, we provide evidence that an oscillatory motion can indeed be generated in the Franck−Condon region of the surface (i.e. the region centered on SP and comprising the FC point).

The fact that coherent oscillations are observed in both bR and solution PSBT implies that the associated molecular motions are somehow similar in these different environments. In other words, the bR cavity does not qualitatively alter the shape of the Franck−Condon region of the retinal chromophore. This conclusion is also supported by resonance Raman spectra analysis, which suggests that the characters of the force fields controlling the initial excited-state dynamics of PSB11 under isolated conditions and inside the Rh cavity are similar.[13,47−49] (In fact, a resonance Raman study of the excited state of bR[50,51] also indicates that the initial relaxation of its PSBT chromophore involves skeletal stretchings, as seen in the isolated systems.) If this is true, the *two-mode* reaction coordinate of **1** (see Scheme 1) should provide a general model for understanding such dynamic features. More specifically, the analysis of this coordinate indicates that the initial part of the photoisomerization path is dominated by stretching modes. Remarkably, a series of different femtosecond time-resolved spectroscopic studies on bR[28,29,52−55] and, more recently, on Rh[13,24] provide evidence that this is indeed the case. Ottolenghi, Ruhman, et al.[28] showed

(45) Kasha, M. *Discuss. Faraday Soc.* **1950**, *9*, 14.
(46) Ruhman, S.; Hou, B.; Friedman, N.; Ottolenghi, M.; Sheves, M. *J. Am. Chem. Soc.* **2002**, *124*, 8854.
(47) Mathies, R.; Freedman, T.; Stryer, L. *J. Mol. Biol.* **1977**, *109*, 367.
(48) Loppnow, G. R.; Mathies, R. A. *Biophys. J.* **1988**, *54*, 35.
(49) Palings, I.; Pardoen, J. A.; Vandenberg, E.; Winkel, C.; Lugtenburg, J.; Mathies, R. A. *Biochemistry* **1987**, *26*, 2544.
(50) Song, L.; El-Sayed, M. A. *J. Am. Chem. Soc.* **1998**, *120*, 8889.
(51) Myers, A. B.; Harris, R. A.; Mathies, R. A. *J. Phys. Chem.* **1983**, *79*, 603.
(52) Zhong, Q.; Ruhman, S.; Ottolenghi, M.; Sheves, M.; Friedman, N.; Atkinson, G. H.; Delaney, J. K. *J. Am. Chem. Soc.* **1996**, *118*, 12828.

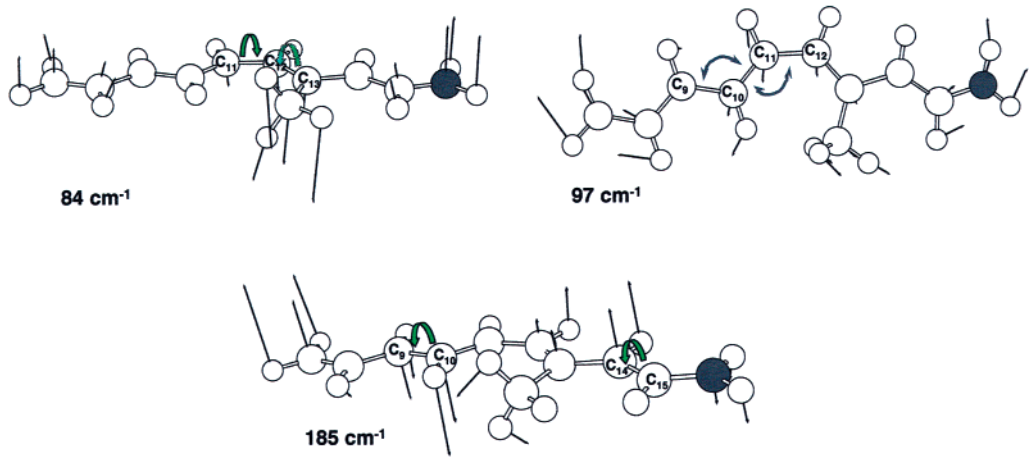

Figure 4. Schematic representation of the three CASSCF low-frequency modes at 84, 97, and 185 cm^{-1} (unscaled frequencies), which are closer to the damped low frequency (~150 cm^{-1}) vibrational coherence observed on S_1. The motion is displayed via vectors on the planar SP structure. The 84 and 185 cm^{-1} modes are dominated by twisting deformations. The 97 cm^{-1} mode corresponds to a totally symmetric bending mode.

that the initial ultrafast (≤100 fs) spectral changes observed in native bR are virtually identical with those recorded for a bR-like receptor containing a modified PSBT chromophore (PSB5.12)

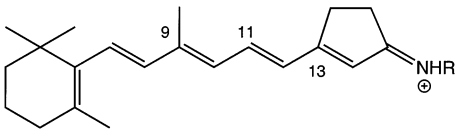

PSB5.12

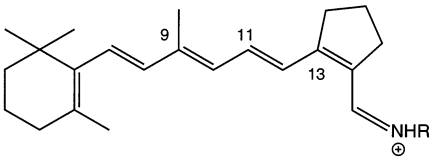

PSB5.13

featuring a five-membered ring moiety locking the biologically active C_{13}═C_{14} double bond. This finding showed that the initial excited-state dynamics is invariant for the unmodified and modified protein, despite the increased torsional rigidity, and suggests that the initial dynamics is driven by other modes (e.g. stretchings).

Since C−C stretching modes are responsible for the early dynamics driving the system out of the FC point, our model suggests that impulsive excitation may lead to coherent wave packet vibrations along these coordinates. However, two observations suggest that the oscillations may involve additional modes. First, while Zinth et al.[30] observed recurrences in C−C stretching modes, Ruhman and co-workers[27−29,46] measured a 156 and 137 cm^{-1} oscillatory frequency (i.e. much below the frequency for a typical C−C stretching) for the native and PSB5.12 locked bR, respectively. The same type of damped oscillation was measured for PSBT and for the 13-cis locked chromophore PSB5.13 in solution, featuring in both cases a 117 cm^{-1} frequency. This indicates that low-frequency modes (such as torsions or skeletal deformations), and not only stretching modes, are readily (≤100 fs) populated in bR and PSBT. Second, the oscillatory feature only appears after an "induction time", not immediately after excitation, suggesting that population of the active modes must follow the very initial excited-state relaxation.

The shape of the Franck−Condon region computed for **1** (as well as for a corresponding PSBT model)[3−5,11] suggests that a low-frequency excited-state wave packet oscillatory motion could be observed near SP (near the planar S_1 configuration of the chromophore) soon after the initial stretching relaxation (i.e. before evolution toward CI) and prior to full internal vibrational energy redistribution. Indeed, as illustrated in Scheme 1, a flat energy plateau comprising a small barrier (<1 kcal mol^{-1}) has been located (see Figure 1 and Table 1).[19] Notice that this plateau, which is entered via evolution along a S_1 low-frequency mode of SP, is held responsible for the slower S_1 isomerization dynamics observed in solution with respect to the protein environment.[5] Indeed, we suggested that in the protein the plateau is significantly reduced in length, thus speeding up the evolution toward the CI decay channel.

The observed low frequency (ca. 120−150 cm^{-1}) oscillations indicate motion of a large portion of the absorbing chromophore along a flat energy surface. The results of a CASSCF frequency computation at SP can be used to characterize the topography of the S_1 PES in the relevant region and provide information on the exact nature of the low-frequency modes. The result reveals that the lowest frequency C−C stretching mode occurs at about 1000 cm^{-1} (consider that the S_1 surface is flatter than the ground-state PES). On the other hand, only three modes at 84, 97, and 185 cm^{-1} can be tentatively assigned[56] to the observed excited-state oscillations (see Figure 4), as the other normal modes are too high in frequency. The vectors displayed in Figure 4 shows that the 84 and 185 cm^{-1} modes correspond to out-of-plane skeletal deformations dominated by twisting components. In contrast, the 97 cm^{-1} mode corresponds to an in-plane skeletal deformation dominated by bending components. Of course, model **1** cannot provide an unambiguous assignment of the observed 117 cm^{-1} (solution) or 156 cm^{-1} (bR) frequencies. In particular, one cannot exclude that the structural difference between PSBT, PSB11, and model **1** yields

(53) Haran, G.; Wynne, K.; Xie, A. H.; He, Q.; Chance, M.; Hochstrasser, R. M. *Chem. Phys. Lett.* **1996**, *261*, 389.
(54) Kobayashi, T.; Saito, T.; Ohtani, H. *Nature* **2001**, *414*, 531.
(55) Haacke, S.; Vinzani, S.; Schenkl, S.; Chergui, M. *CHEMPHYSCHEM* **2001**, *2*, 310.
(56) The reported CASSCF frequency values are unscaled.

Table 4. Energy Gap and Oscillator Strengths (f)[a] for Radiative S_1-S_0 Transitions (Absorption/Emission) at Selected Points along the Three Lowest (84, 97, and 186 cm^{-1}) S_1 Vibrational Modes Computed at Structure SP

		84 cm^{-1} Mode			
displacement (au)	SP	1.6	3.2	4.9	6.5
S_1-S_0 (nm)	602	606	613	624	639
f	1.05	1.05	1.04	1.03	1.01
		97 cm^{-1} Mode			
displacement (au)	SP	1.6	3.2	4.7	6.3
		(−1.6)	(−3.2)	(−4.7)	(−6.3)
S_1-S_0 (nm)	602	610	620	633	649
		(597)	(594)	(593)	(595)
f	1.05	1.04	1.03	1.01	0.99
		(1.05)	(1.05)	(1.04)	(1.03)
		185 cm^{-1} Mode			
displacement (au)	SP	1.7	2.5	3.3	4.2
S_1-S_0 (nm)	602	605	609	616	624
f	1.05	1.04	1.03	1.04	0.98

[a] See ref 33.

significantly different frequency values. The 97 cm^{-1} bending is dominated by changes at the $C_9-C_{10}-C_{11}$ and $C_{10}-C_{11}-C_{12}$ angles. The lowest energy frequency mode is dominated by twisting about the central $C_{11}-C_{12}$ and, to a lesser extent, about the $C_{12}-C_{13}$ bonds. Furthermore, this mode correlates with the reaction coordinate (i.e. motion along this mode would displace the molecule along the S_1 energy plateau discussed above). In contrast, the 185 cm^{-1} mode is dominated by twisting about the C_9-C_{10} and $C_{14}-C_{15}$ bonds. Note that since none of these deformations are enclosed in the five-membered-ring lock of PSB5.12, one expects only small effects of the lock on the frequency of the modulation.

In Table 4 we report the effect of the displacement of the SP equilibrium structure along the 84, 97, and 185 cm^{-1} modes on the S_1-S_0 energy gap and oscillator strength. Considering that the geometrical displacement of ca. 6.5 au approaches the maximum allowed energy increase (i.e. the S_1 energy difference between FC and SP), both the 84 and 185 cm^{-1} torsions lead to a slight decrease of the energy gap (corresponding to a ca. 35 nm increase in the absorption wavelength) and oscillator strength. These variations may be responsible for the observed modulation in the stimulated emission intensity. The 97 cm^{-1} bending mode displays an only slightly larger effect.

While the computed 84 cm^{-1} mode is a possible candidate for the assignment of the observed oscillatory motion, the molecular mechanism that leads to fast population of this mode, presumably starting from an impulsively populated stretching mode, and, most importantly, the apparent nonperiodicity of the observed oscillatory motion remain without an even tentative explanation. Below we show that the structure of the Franck−Condon region of **1** provides such an explanation when classical trajectories are investigated in that region.

A crude two-dimensional analytical model ($V(x_S,y_T) = a_S x_S^2 + (b_T x_S) y_T^2$) of the Franck−Condon region centered at SP is given in Figure 5a. Consistent with our computations, the model includes a totally symmetric harmonic "stretching" mode (x_S) and an orthogonal nontotally symmetric "torsional" mode (y_T). Notice that the curvature along the torsional mode is a function of the stretching coordinate and changes from positive (near the FC point) to negative (beyond SP). As mentioned above, this topography of the Franck−Condon region is supported by CASSCF frequency computations on different model systems.[11]

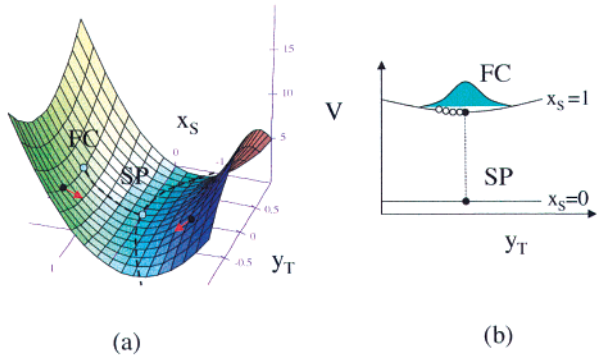

Figure 5. (a) Plot of the model S_1 potential $V(x_S,y_T) = a_S x_S^2 + (b_T x_S) y_T^2$ with $a_S = 6$ and $b_T = 3$. x_S is associated with a totally symmetric stretching. y_T is associated with a torsional deformation about the 11-cis double bond. The dashed lines indicate the position of the photoisomerization path. Note that this path bifurcates at SP consistently with the CASSCF path of model **1**. The arrows indicate the "attractive" (left, concave potential) and "repulsive" (right, convex potential). (b) Schematic representation of the vibrational wave packet cross-section along y_T at FC. The circles indicate the positions where a series of classical trajectories (see text) are released.

Scheme 3

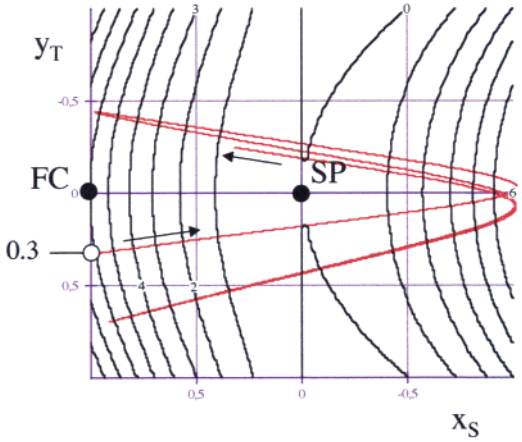

Thus, at time zero (i.e. near FC), any nonplanar configuration belonging to the initial vibrational wave packet will "feel" a force pointing toward the bottom of the valley (i.e., to a planar configuration). On the other hand, after $^1/_4$ stretching oscillation (i.e. along x_S) the configuration will feel a force pointing away from planarity, since the curvature along y_T is now negative. For this reason one expects that, due to the S_1 energy surface topography, a number of trajectories will be accelerated back and forth along the torsional mode every $^1/_2$ stretching oscillation. This concept is illustrated in Scheme 3 on the basis of the contour diagram of the surface of Figure 5a. Because of the initial symmetry of the wave packet, this motion will appear as an alternate contraction and expansion of the wave packet along the torsional coordinate y_T.

The model given above can be used to look at the behavior of a set of classical trajectories released near FC. In particular, the trajectories released from points displaced along the twisting coordinate y_T (see Figure 5b) provide a crude model of the cross-section of the wave packet along the torsional coordinate. The values of the parameters a_S and b_T (see caption to Figure 5) have been chosen to mimic the topography of the computed PES. Thus, FC is placed ca. 10 kcal mol^{-1} higher in energy than SP and at a distance of 1 au (interpreted as a distance in mass-weighted coordinates) from SP. Furthermore, at FC, the

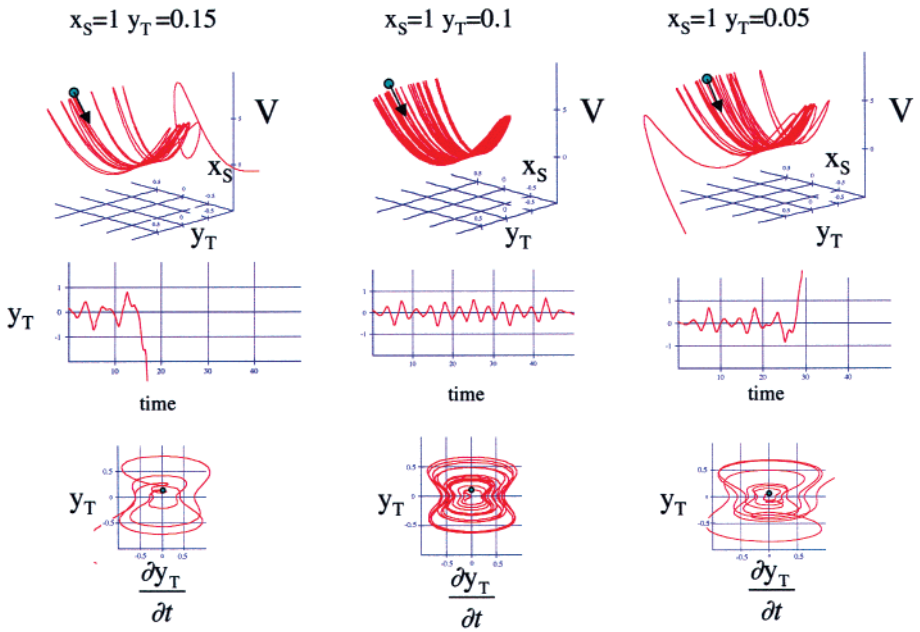

Figure 6. (top) Space curves of the three types of trajectories discussed in the text and corresponding to the following pairs of initial conditions (right to left): $x_S = 1$, $y_T = 0.5$; $x_S = 1$, $y_T = 1.0$; $x_S = 1$, $y_T = 1.5$. In all cases the initial velocities are set to zero. The circle indicates the starting point in the vicinity of FC. (middle) Corresponding diagrams illustrating the oscillations along y_T as a function of time. The nonperiodicity of the motion is apparent. Note that the frequencies are approximately the same for the three trajectories. (bottom) Associated phase-space diagrams for the torsional coordinate y_T.

surface curvature along y_T has been set to be $^1/_2$ of the surface curvature along x_S to mimic the flatter nature of the twisting mode. In Figure 6 we show the behavior of three different classical trajectories released near FC with no initial kinetic energy. These trajectories are characterized by the value of the y_T "torsional" displacement from the symmetrical structure FC (i.e. 0.05, 0.1, and 0.15 au). Note that the 0.1 au trajectory oscillations remain permanently confined in the Franck−Condon region (as shown by the corresponding phase space diagram).

Note also that the modulations appear to be quasi-periodic, as the shape of each oscillation changes slightly with time. In contrast, trajectories starting from a point displaced slightly less (0.05 au) and more (0.15 au) oscillate only for a finite time and then escape the Franck−Condon region along the flat "torsional" y_T mode. This rather sudden change of regime from "stable" to "unstable" motion occurs for different values of the initial displacement. In Figure 7 we report the "lifetime" of a set of trajectories as a function of the initial displacement from FC. It is clear that trajectories which start close to the 0.1 and 0.3 au displacements generate stable (or long-lived) "orbits". In the other ranges (e.g. in the region of 0.05, 0.2, and 0.35 au) the computed trajectories are short-lived. Thus, our crude excited-state energy surface model suggests that the original wave packet should decay according to (at least) two different regimes. In other words, the wave packet would split into two populations decaying with a slower and a faster time scale, leading to a multiexponential decay. The nonperiodic character of the oscillations and the existence of multiple decay regimes are consequences of the nonharmonicity of the excited-state energy surface. In fact, the cubic term $x_S y_T^2$ of $V(x_S,y_T)$ leads to a system of equations of motion corresponding to a fourth-order nonlinear dynamical system.[57] It is well-known that such a system leads, in contrast to linear systems, to qualitatively different classes of trajectories such as quasi-periodic and chaotic trajectories.

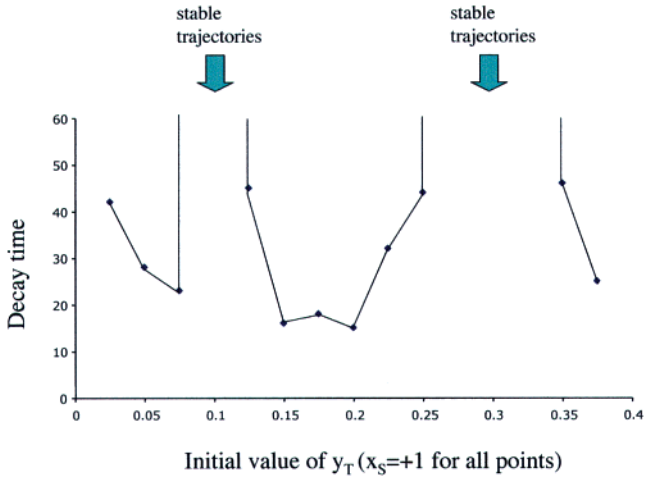

Figure 7. Decay times (defined as the time when y_T reaches a 1.5 displacement) as a function of the initial conditions. The lowest initial y_T value is 0.025, and the largest is 0.375. x_S is kept fixed at the value of 1. The points are separated by a 0.025 interval.

Another potential energy feature that allows for the existence of different dynamics regimes is the symmetry of the potential with respect to the y_T torsional coordinate. This is a consequence of the planar structure of the PSB11 model **1** at SP. However, in the protein cavity PSB11 will not be planar, as the molecular environment is chiral and the symmetry of the S_1 energy surface is lost. In this case, a qualitatively correct model potential for the Franck−Condon region is $V(x_S,y_T) = a_S x_S^2 + (b_T x_S) y_T^2 + c_T y_T$, where the energy surface is sloped along the y_T variable. The $c_T y_T$ term will prompt acceleration toward clockwise or counterclockwise torsional deformation, depending on the sign of the c_T constant. Computation of the classical trajectories, defined by the same set of initial conditions used above, allows

(57) Percival, I.; Richards, D. *Introduction to Dynamics*; Cambridge University Press: London, 1982.

for the study of the effect of the slope on the initial dynamics of the system. The analysis of the trajectories computed for a small slope ($c_T = 0.1$) suggests that the Franck−Condon dynamics are now characterized by a single regime as all trajectories (i.e. from 0.05 to 0.375 displacement along y_T) rapidly decay. Thus, our crude analytical model suggests that a sloped (torsionally asymmetric) energy surface is consistent with a monoexponential decay. Even if, once again, the two-dimensional models presented here have to be considered crude models of the retinal PSB chromophore in different environments, it is encouraging that the decay of the stimulated emission signal observed in solution PSBT is biexponential, while that observed in bR is monoexponential.[19,20,27] In the past, tentative explanations for the observed biexponential decay of solution PSB have been proposed to involve the presence of two different conformers as well as the involvement in the decay of two different excited states. The dynamics model discussed above provides a third possible explanation.

Conclusions

In the past[4,5] we have shown that the computationally derived *two-state/two-mode* model for the photoisomerization path of retinal chromophores provides a rationalization of the *initial* S_1 relaxation dynamics of these chromophores, either in solution or in the opsin cavity.[13,19,20,24,28−30,47−49,53] In the present paper we show that the same reaction coordinate model, as well as the associated PES topography, can be used as a basis for the (qualitative) understanding of (i) the excited-state absorption and emission seen in different retinal PSBs, (ii) the $S_2 \rightarrow S_1$ radiationless decay, and (iii) the excited-state dynamics following initial relaxation and leading to spectral modulations.

Regarding point i, we have employed a CASPT2//CASSCF strategy to describe the single manifold (up to the fifth root) for the retinal PSB11 model **1** along the initial part of its 11-cis → all-trans photoisomerization path. The results (see Figure 1) show that the $S_1 \rightarrow S_4$ transition can be tentatively assigned to the observed excited-state absorption in solution, while the $S_1 \rightarrow S_3$ transition may correspond to the excited-state absorption observed in bR when a crude hypothesis on the origin of the opsin shift is considered. The same hypothesis also explains the competing near-IR absoption (assigned to the $S_1 \rightarrow S_2$ transition) and emission (assigned to the $S_1 \rightarrow S_0$ transition) observed in bR.

The characterization of a planar low-lying S_2/S_1 conical intersection funnel in our PSB11 model (point ii above) suggests that ultrafast $S_n \rightarrow ... \rightarrow S_1$ deactivation of PSB chromophores may occur along a series of low-lying conical intersections interconnecting the relevant singlet excited states. This hypothesis is currently under investigation in our laboratory.

Finally, a crude classical model has been proposed for the investigation of the decay dynamics and oscillatory features observed in bR, PSB5.12 locked bR, and solution PSBT. It is concluded that the origin of the oscillatory features could be ascribed to nonlinear dynamics occurring on the highly anharmonic PES of PSBs. The same model seems to explain the origin of the experimentally observed biexponential decay of PSBT in solution. The different decay regimes would be due to groups of stable and unstable trajectories that originate in the FC region of the S_1 PES.

Acknowledgment. We kindly acknowledge the very fruitful discussion with Prof. Sandy Ruhman. Funds have been provided by the Università di Siena (Progetto di Ateneo A.A. 02/04), HFSP (RG 0229/2000-M), MURST (Cofin 2000, Cofin 2001 and 60%), and the Alma Mater Studiorum − University of Bologna (Funds for Selected Topics). We wish to thank "Cineca" for granted calculation time on their computers.

Supporting Information Available: Tables giving the Cartesian coordinates of all structures discussed in the text. This material is available free of charge via the Internet at http://pubs.acs.org.

JA030215J